Knot theory realizations in nematic colloids

Simon Čopar[a,1], Uroš Tkalec[b,c,1,2], Igor Muševič[a,b], and Slobodan Žumer[a,b]

[a]Faculty of Mathematics and Physics, University of Ljubljana, 1000 Ljubljana, Slovenia; [b]Jožef Stefan Institute, 1000 Ljubljana, Slovenia; and [c]Faculty of Natural Sciences and Mathematics, University of Maribor, 2000 Maribor, Slovenia

Edited by Tom C. Lubensky, University of Pennsylvania, Philadelphia, PA, and approved December 29, 2014 (received for review September 5, 2014)

Nematic braids are reconfigurable knots and links formed by the disclination loops that entangle colloidal particles dispersed in a nematic liquid crystal. We focus on entangled nematic disclinations in thin twisted nematic layers stabilized by 2D arrays of colloidal particles that can be controlled with laser tweezers. We take the experimentally assembled structures and demonstrate the correspondence of the knot invariants, constructed graphs, and surfaces associated with the disclination loop to the physically observable features specific to the geometry at hand. The nematic nature of the medium adds additional topological parameters to the conventional results of knot theory, which couple with the knot topology and introduce order into the phase diagram of possible structures. The crystalline order allows the simplified construction of the Jones polynomial and medial graphs, and the steps in the construction algorithm are mirrored in the physics of liquid crystals.

liquid crystal colloids | knot theory | topological defects | knotted fields

From the invention of ropes and textiles, up to the present day, knots have played a prominent role in everyday life, essential crafts, and artistic expression. Beyond the simple tying of strings, the intriguing irreducibility of knots has led to Kelvin's vortex model of atoms, and, subsequently, a more systematic study of knots and links in the context of knot theory (1–3). As a branch of topology, knot theory is a developing field, with many unresolved questions, including the ongoing search for an algorithm that will provide an exact identification of arbitrary knots.

As knots cannot be converted one into another without the crossing of the strands—a discrete singular event—knotting topologically stabilizes the structure. In physical fields, this coexistence of discrete and continuous phenomena leads to the stabilization of geometrically and topologically nontrivial high-energy excitations (4, 5). Examples of strand-like objects in physics that can be knotted include vortices in fluids (6–9), synthetic molecules (10, 11), DNA, polymer strands and proteins (12–14), electromagnetic field lines (15, 16), zero-intensity loci in optical interference patterns (17), wave functions in topological insulators (18), cosmic strings (19), and defects in a broad selection of ordered media (20–23).

Nematic liquid crystals (NLC) are liquids with a local apolar orientational order of rod-like molecules. The director field, which describes the spatial variation of the local alignment axis, supports topological point and line defects, making it an interesting medium for the observation of topological phenomena (20, 24). Defect structures in NLC and their colloidal composites (25) have been extensively studied for their potential in self-assembly and light control (26), but also to further the theoretical understanding of topological phenomena in director fields (23, 27). Objects of interest include chiral solitons (28, 29), fields around knotted particles (30–35), and knotted defects in nematic colloids (36–42). Each of these cases is unique, as the rules of knot theory interact with the rules and restrictions of each underlying material and confinement. The investigation of knotted fields is thus a specialized topic where certain theoretical aspects of knot theory emerge in a physical context.

In nematic colloids—dispersions of spherical particles confined in a twisted nematic (TN) cell—disclination lines entangle arrays of particles into "nematic braids," which can be finely controlled by laser tweezers to form various linked and knotted structures (38, 39, 43). In this paper, we focus on the diverse realizations of knot theory in such nematic colloidal structures. We complement and extend the classification and analysis of knotted disclinations from refs. 32, 38, 40 with the direct application of graph and knot theory to polarized optical micrographs. We further analyze the nematic director with constructed Pontryagin–Thom surfaces and polynomial knot invariants, which enables a comprehensive topological characterization of the knotted nematic field based on experimental data and analytical tools. We use a λ-retardation plate to observe and distinguish differently twisted domains in the optical micrograph, which correspond to medial graphs of the represented knots and contribute to the Pontryagin–Thom construction of the nematic director. Finally, we explore the organization of the space of possible configurations on a selected rectangular particle array and discuss the observed hierarchy of entangled and knotted structures.

Colloidal Arrays, Knot Projections, and Tangles

We observe the TN cell with dispersed microparticles under the polarizing optical microscope (POM), sandwiched between crossed polarizers. Due to the light scattering on the defect core, the disclinations (line defects) in the nematic order that form around the particles are clearly visible and trace out a knot diagram (1, 2), as demonstrated in Fig. 1. In the projection seen by the microscope, we observe only two types of crossings: at each particle, the top and bottom disclinations cross perpendicularly; in the space between four neighboring particles there is a point where the disclinations can also cross, but they can also bypass one another. The experimental image thus constitutes a knot diagram, which is all of the information needed to further analyze the topology of the knot formed by the disclination loops (Fig. 1 *D*–*F*).

The NLC between the particles can be manipulated with laser tweezers to switch between different entangled states. These so-called "tangles" are top projections of the three different configurations of a rewiring site where two disclination segments approach closely in a tetrahedrally shaped formation (40). The possible tangles are the crossing tangle  and the smoothings  and (Fig. 1*E*). These tangles exactly correspond

Significance

Knot theory is a branch of topology that deals with study and classification of closed loops in 3D Euclidean space. Creation and control of knots in physical systems is the pinnacle of technical expertise, pushing forward state-of-the-art experimental approaches as well as theoretical understanding of topology in selected medium. We show how several abstract concepts manifest elegantly as observable and measurable features in nematic colloids with knotted disclination lines. Construction of medial graphs, surfaces, and Jones polynomials is showcased directly on experimental images, and adapted for the specific system of colloidal crystals in a twisted nematic cell. Discussing the correspondence between topological concepts and experimental observation is essential for building the bridge between mathematical and physical communities.

Author contributions: U.T. and I.M. designed research; S.Č. and U.T. performed research; S.Č., U.T., and S.Ž. analyzed data; and S.Č., U.T., I.M., and S.Ž. wrote the paper.

The authors declare no conflict of interest.

This article is a PNAS Direct Submission.

[1]S.Č. and U.T. contributed equally to this work.

[2]To whom correspondence should be addressed. Email: uros.tkalec@ijs.si.

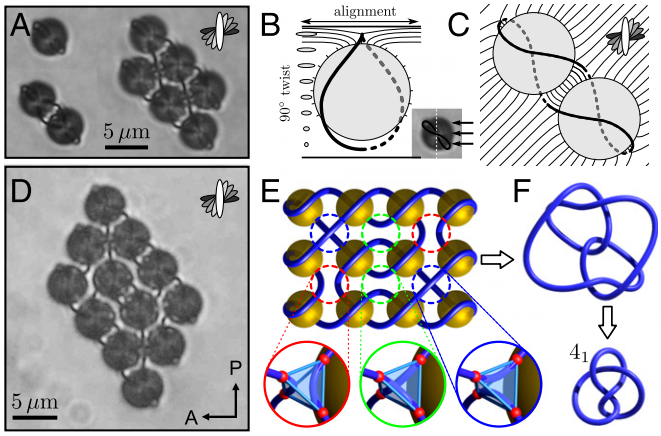

Fig. 1. (*A*) Polarized optical micrographs of a single Saturn-ring structure, an entangled dimer, and an entangled cluster of particles with a homeotropic surface anchoring in a right-handed 90° TN cell. (*B*) Side view of the director field and disclinations in the Saturn-ring structure from *A* showing the effect of a 90° twist. (*Inset*) Direction of view. (*C*) Sketch of the director streamlines around the dimer in a horizontal midplane cross-section. Notice the disclinations delimit opposite twist domains with perpendicular midplane director orientation. (*D*) Example of disclinations entangling a 4×3 array of particles. (*E*) Idealized and rectangularly aligned depiction of a knot diagram for the structure in *D*. The tangles between four adjacent particles can exist in three different states, which can be individually switched with laser tweezers. (*F*) Topology-preserving simplification of the disclination geometry in *E* identifies a figure-eight knot (4_1).

to the tangles studied in knot theory and enter the knot invariants via Skein relations (1), which we will exploit later.

The relationship between the 3D nematic field and the projected knot diagrams ensures that in the TN cell, we observe exactly these three tangles at the positions between the particles in a grid. Due to the alignment of the TN director field at the bottom and top plate of the cell, there is only one type of crossing, which simplifies the calculations and restricts the set of possible knot diagrams on a selected grid size. Depending on how the tangles are configured, the disclinations can form different knots or links, which are limited in complexity only by the size of the colloidal aggregate (38, 39). The curve traced by the disclination can be extracted directly from the experimental image and either identified by hand, or simplified with specialized software (44) to detect which particular knot or link is formed (Fig. 1*F*). However, the geometric restrictions based on the physics of the containing TN cell lead to interesting properties that allow a more elegant investigation of the knotted structures.

Twist Domains and Medial Graphs

An intriguing feature of entangled colloidal structures in a TN cell is the microscopic twist domains locked between the colloidal particles and the defects. Adjacent twist domains, separated by disclinations, have opposite handedness and their director field orientation in the cell midplane differs by 90° (Figs. 1*C* and 2*A*). The twist domains of opposite handedness are, in the absence of intrinsic chirality of the NLC, degenerate in free energy. When observing a large entangled colloidal crystal between crossed polarizers with an inserted λ-plate (45), the oppositely twisted domains appear as blue-green– and yellow-gray–colored regions (Fig. 2). The colors are caused by the difference in the angle between the average director orientation inside a particular domain and the orientation of the λ-plate. Minor color differences between the samples are caused by small variations in the cell thickness.

The twist-domain colors are related to graph theory. A duality between the knot diagrams and edge-signed planar graphs implies a knot projection can alternatively be represented as a graph. A knot projection delimits space into "faces" that can be alternately colored with two different colors. The vertices (nodes) of the graph represent the enclosed faces of one color, and the graph edges represent the crossings between the faces (1). Two-dimensional, entangled, colloidal structures in a NLC provide a natural framework for the construction of a planar graph from the projection of the entangled defect loops and the colored domains among them (Fig. 2). We assign a graph vertex to each same-colored region and connect adjacent regions with edges. Each graph edge is labeled as "+" or "−" depending on the type of the crossing it passes through Fig. 2*D*). The result is a signed planar graph, a medial graph of the knot diagram.

Every tangle rewiring is a local operation that does not change the global alternating color pattern, but only connects or

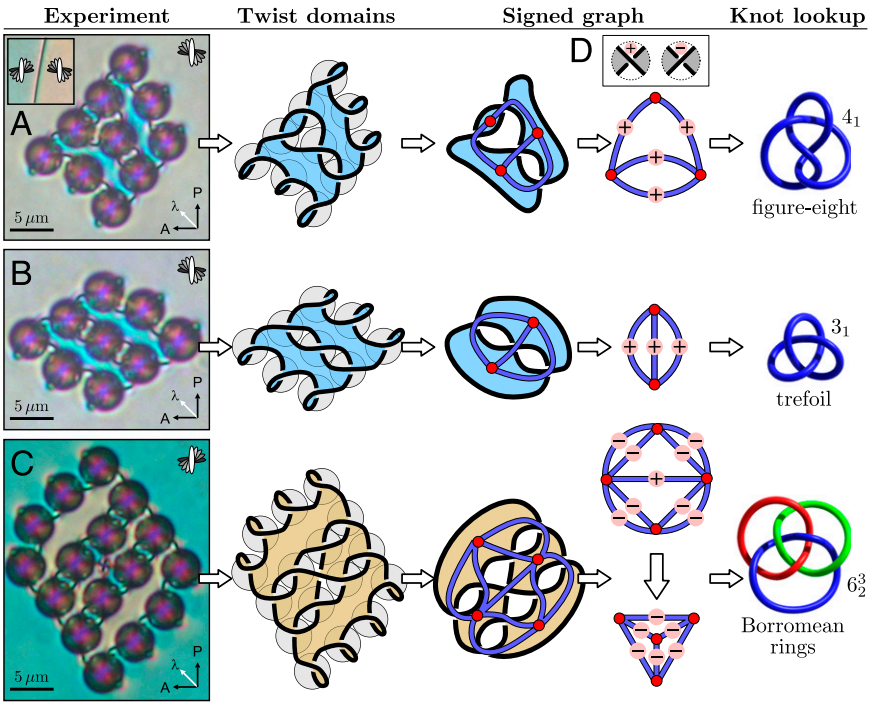

Fig. 2. Entangled colloidal aggregates show alternating colored domains, delimited by the disclinations. (*A*) The grid does not have to be rectangular to construct the graph. The cell in *C* has an opposite handedness compared with *A* and *B*. (*A*, *Inset*) Interface between chiral domains of opposite handedness. A λ-plate oriented at 45° to both polarizer and analyzer reveals the domains in different colors. The colored domains map directly to the nodes of the medial graph. (*C*) The resulting signed planar graph can be further simplified with the graph version of the Reidemeister moves and used to recognize the knot. (*D*, *Inset*) The graph edges are labeled as "+" or "−" according to the type of crossing they represent. The structures in the panels are the figure-eight knot (4_1), the trefoil knot (3_1), and the Borromean rings (6_2^3), respectively.

disconnects the color domains. The edges that correspond to the disclination crossings seen at the particles all have one sign, whereas the edges corresponding to the ⨯ tangles have the opposite (Fig. 2 *C* and *D*). This makes the graph construction easier: not only are the colors given by the experiment, but the edge signs can be immediately filled in without checking their orientations individually.

The medial graph is ideal for a straightforward calculation of the Göritz matrix and, subsequently, the knot signature and determinant, which for nematics also helps to determine the number of distinct director field textures (34). The resulting graph can be further simplified by the Reidemeister moves adapted for the graph representation (1). Thus, a simplified graph can be constructed and then used to identify the knot or link from a lookup table, or with a calculation of further invariants. The graph can be constructed even if the colloidal array is not rectangular, and works for any colloidal aggregate bound by disclinations (Fig. 2).

Pontryagin–Thom Construction

The colored region extracted from the λ-plate micrographs can also be considered a top projection of a surface bounded by the disclinations (Fig. 3). At the crossings, this surface contains "twisted bands," where the surface turns the other side toward the observer. An important topological invariant, the Euler characteristic, is obtained from the colored region as $\chi = b - t - v$, where b is the number of rows in an $a \times b$ array of particles, whereas t and v are the numbers of ⨯ and) (tangles, respectively. The expression encodes the fact that the ⨯ and) (tangles add additional bands to the surface. The surface is only orientable if the medial graph associated with the same colored region is bipartite—if it contains no odd cycles (for an odd cycle, see Fig. 3*B*). In the orientable case, the surface is a Seifert surface of the knot and can be used to extract topological properties via the Seifert matrix, such as the knot signature, Alexander polynomial, the upper bound of the knot's genus, and the lower bound on the unknotting number (3).

Regardless of its orientability, the extracted surface can also be used to construct the Pontryagin–Thom (P-T) surface—a surface that compactly, but uniquely, describes the nematic texture up to a smooth topology-preserving transformation (29). It is defined as the surface where the director field lies in a plane perpendicular to the far-field orientation, and colored by the angle of the director in this plane (Fig. 3 *B* and *D*). In general, the definition of the far-field director is ambiguous in a TN cell, but for a 90° twist, taking the far field at the middle of the cell as a reference direction (*y* direction in Fig. 3), it is only a minor and topologically insignificant simplification.

The alternating nature of the director orientations of the twist domains between the colloidal inclusions implies that the P-T surface in the top projection coincides with the colored regions in the λ-plate micrographs as can be seen in Fig. 3 *A* and *B*. This fixes the shape of the surface up to a homotopy, but not the colors representing the precise director orientation. Without experimentally or numerically provided director field information, we predict the director based on the fact that around $-1/2$ disclination it lies perpendicular to the disclination tangent. Near the disclination itself, the representative direction can be extracted as an intersection of the reference plane and the plane, perpendicular to the disclination. Away from the defects, the color interpolation is continuous and unique up to a homotopy, which allows a sketch of the surface. The surfaces in Fig. 3 were constructed by solving a Laplace equation with the color and position defined at the disclination lines. Idealized shapes of the disclinations were modeled with the splines of circular arcs, as used already for the visualization in ref. 38.

The P-T surface is bounded by line and point defects in the system, and for the point defects, the number of turns of the "color wheel" measures the topological charge. The surface acts as a reference that connects point and line defects that together amount to a zero total topological charge. The defects and particles that are topologically bound together with the same P-T surface cannot be separated without remaining tethered or

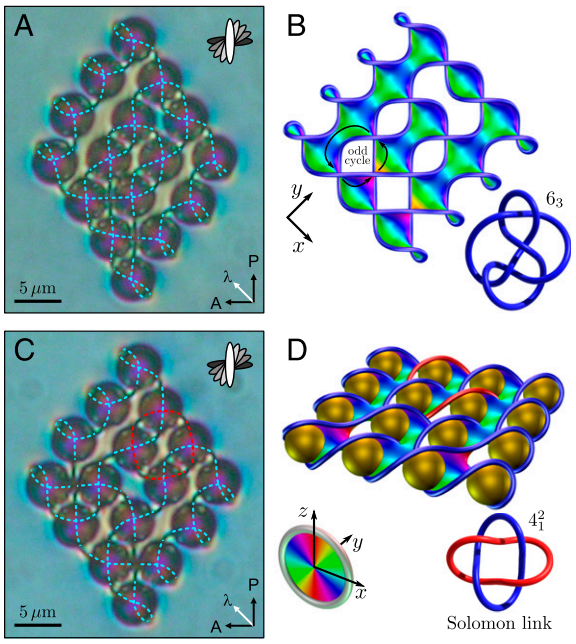

Fig. 3. (*A* and *C*) Experimental λ-plate micrographs of nematic braids that form the 6_3 knot and the Solomon link, respectively. The disclinations at the colloidal particles are traced with dashed lines for visual guidance. (*B* and *D*) Geometrically idealized, but topologically accurate P-T surfaces for the structures in *A* and *C*. The surface locates where the director is perpendicular to the far field at midheight (*y* direction). The colors encode the direction within this plane (*D*, *Inset*, *Left*). *B* omits the particles to pronounce the regular shape of the surface. *D* shows the P-T surface for structure *C* in perspective. Note the red shading at the cross-tangles that signifies vertical director field.

undergoing a discontinuous rearrangement. The "topological entanglement" defined in this way matches the intuitive notion of entanglement. The disclinations ensure that the entire cluster of particles is topologically irreducible, in contrast with the more common situation, where the point defects, particles, and disclinations are bound up into neutral pairs, which in turn interact weakly via residual elastic interactions (26, 46, 47).

This approximate construction retrieves a topologically exact P-T surface without using any director field information, simply by inferring the disclination orientation from the experimental image. The resulting surface can be used to further investigate the topological properties of the knot, and in particular, the director texture that lies in the knot complement (34). Such a classification is more precise, as two isotopic knots may have a topologically distinct director field around them.

Polynomial Invariants

The examples above focused on individual structures and could be analyzed by hand. However, a robust and automated knot classification is needed to analyze the entire multitude of possible knots on a selected lattice. For that purpose, we use polynomial knot invariants, which are easily calculable from the tangle representation via the Skein relations (1, 2). A particularly suitable choice is the Kauffman bracket polynomial, because it does not require an oriented knot diagram (48). In this section, we shortly summarize the routine, adapted to the geometry of colloidal lattices, first developed for the classification of knots in ref. 38.

The computation of the Kaufmann bracket boils down to a recursion that relates a particular knot projection to modified projections with one crossing replaced by a smoothing. The recursion stops when all of the crossings are removed, leaving a set of unknotted and unlinked loops. A correction factor is required to obtain the Jones polynomial, which is a true topological

invariant (48). A closed-form expression for the Jones polynomial sums over all simplified diagrams

$$X(A) = (-A)^{3w} \sum \left(-A^{-2} - A^{2}\right)^{n-1} A^{u-v}, \qquad [1]$$

where u and v are the number of and tangles that replaced all of the crossings and n is the number of components that build up each specific final configuration with no crossings (Fig. 4) (2). Sometimes the polynomial is expressed in terms of a different variable, $t = A^{-4}$. The correction factor (the integer writhe number w) is extracted from an oriented diagram of the original knot, as a sum of ± 1 contributions over all of the crossings (Fig. 4*D*).

To treat the nematic braids as knot projections, the particles are interpreted as tangles. On the aligned grid, the calculation can be easily automated, but the diagram can first be simplified in several ways. Firstly, the crossings that belong to the leftmost and rightmost column of particles can be removed (Fig. 4*B*). The remaining diagram can be further simplified by performing the grid-aligned counterparts of the Reidemeister moves of the first and second kinds, as demonstrated in Fig. 4 *C* and *D*. These moves can remove a great deal of unnecessary crossings in an $\mathcal{O}(N^2)$ preprocessing pass where N is the number of particles. This is of vital importance because the computational complexity of the Kauffman polynomial is exponential in the number of crossings. For a 4×4 grid, the optimization removed ~ 7 crossings on average and reduced the computation time by a factor of 50.

After the Jones polynomial is obtained, we can find which knot or link a given nematic braid encodes. For knots of low enough complexity, a comparison of the result with databases of known Jones polynomials gives a probable answer, even though the Jones polynomial is not unique for each knot. The hypothesized knot has to be additionally verified using other methods, such as the medial graph analysis we mentioned above. For the knots that are found on colloidal arrays of sizes up to at least 4×4, the Jones polynomial is a reliable and computationally accessible way of determining the knot type (38). Note that with minor modifications, the algorithm can be extended to produce the HOMFLY polynomial, which is a stronger invariant (1).

The nematic braids are related to mirror knots and curves, with an additional constraint of allowing only one type of crossing (49). The above simplifications with Reidemester moves are the counterparts of simplifications for mirror curves, except for the Reidemester move III, which has no easy local realization if there is only one type of crossing. The rectangular layout of the knots resembles Celtic knotwork patterns. They are also examples of Legendrian knots, because the $-1/2$ disclination profile implies that the curve is roughly perpendicular to the helically ordered, far-field director, which forms a standard contact structure (50).

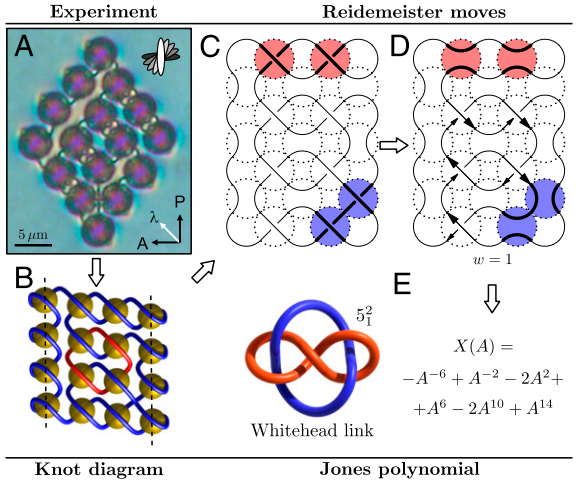

Fig. 4. Extraction of the Jones polynomial on a rectangular colloidal grid. (*A*) POM image of a 4×4 grid with nine active tangles and additional tangles at each particle. (*B*) The end hooks can be trivially ignored before classification (dashed line). (*C* and *D*) Reidemeister moves of I type (red) and II type (blue) are found and resolved in a preprocessing pass. The remaining crossings contribute to the integer writhe w according to the curve orientation. (*E*) The final result of Eq. **1** is the Jones polynomial $X(A)$, which reveals the original structure is the Whitehead link.

Hierarchy of Entangled Arrays

With the reliable classification algorithm described in the previous section, we can observe the structure of the configuration space of all of the knots on a selected lattice. Besides the knot type, the $-1/2$ disclinations present in our system are also characterized by the self-linking number (Sl), a topological invariant that measures the number of intrinsic turns of the profile embedded in the loop (40). The threefold symmetry of the cross-section allows Sl to be an odd multiple of $1/3$ if the loop is linked an odd number of times, and an even multiple of $1/3$ if it is unlinked or linked an even number of times with other components of the link. The Sl also holds partial information about the topological charge q of the system in the form

$$\frac{3}{2}\left(\sum_i \mathrm{Sl}_i + 2\sum_{i>j} \mathrm{Lk}_{ij}\right) + n = q \bmod 2, \qquad [2]$$

where n is the number of components, Sl_i are their self-linking numbers, and Lk_{ij} are the linking numbers between any pair of components (27, 40). The switch of a tangle—a rotation of the tetrahedron at the rewiring site—changes the number of components by 1 and changes the first term on the left-hand side of Eq. **2** by $\pm 2/3$, if the switch can be done without changing orientations in an oriented knot diagram (Fig. 5, detail).

The size of the particle array fixes the topological charge. In a diagram with $\mathrm{Sl} = \sum_i \mathrm{Sl}_i$ and n on its axes, the possible structures that can be generated by different combinations of tangles form a checkerboard grid with linked and unlinked structures in alternating grid cells (38). This approach imparts a partial order to the ensemble of $3^{(a-1)\,(b-1)}$ possible structures on an $a \times b$ array. A switch of one tangle predominantly changes between diagonally adjacent structures, so proximity on the diagram suggests a metric of how many switches are required to change from one knot to the other. However, a switch of a tangle may also jump far across the diagram if the rewiring violates the orientation, so a strict ordering of the diagram is not possible. With an increasing array size, the number of states grows exponentially, so even after ordering them into the (Sl, n) diagram, the number of different knots and links that share the same linking invariants grows quickly. Although this prevents prediction of the knot type based only on the Sl, there is nevertheless an intricate hierarchical structure in the diagrams.

Any array can be constructed by incrementally adding single rows and columns, usually with the use of laser tweezers. Adding a column preserves the knot topology if the added tangles are all of the type (Fig. 5, *Bottom Right*). On the other hand, the addition of a row adds a single unknotted component if all of the new tangles are of the type (Fig. 5, *Top Left*). Changing one of the new tangles into a or tangle attaches the new loop to one of the existing loops, restoring the topology of the original structure. Thus, a larger array includes all of the knots found on smaller arrays (Fig. 5).

The persistence of old structures under the addition of rows or columns results in a hierarchical structure of lower-dimensional subdiagrams contained in larger diagrams. The addition of a row or a column in a topology-preserving way shifts the Sl due to the introduction of an extra plectonemic twist. Every $a \times b$ diagram includes an $(a-1) \times b$ diagram shifted $2/3b$ to the left and several $a \times (b-1)$ diagrams shifted $2/3(a-1) \pm 2/3$ to the left, or by $2/3(a-1)$ to the left and vertically one unit (with a free loop added to the existing topology). Each subdiagram in turn

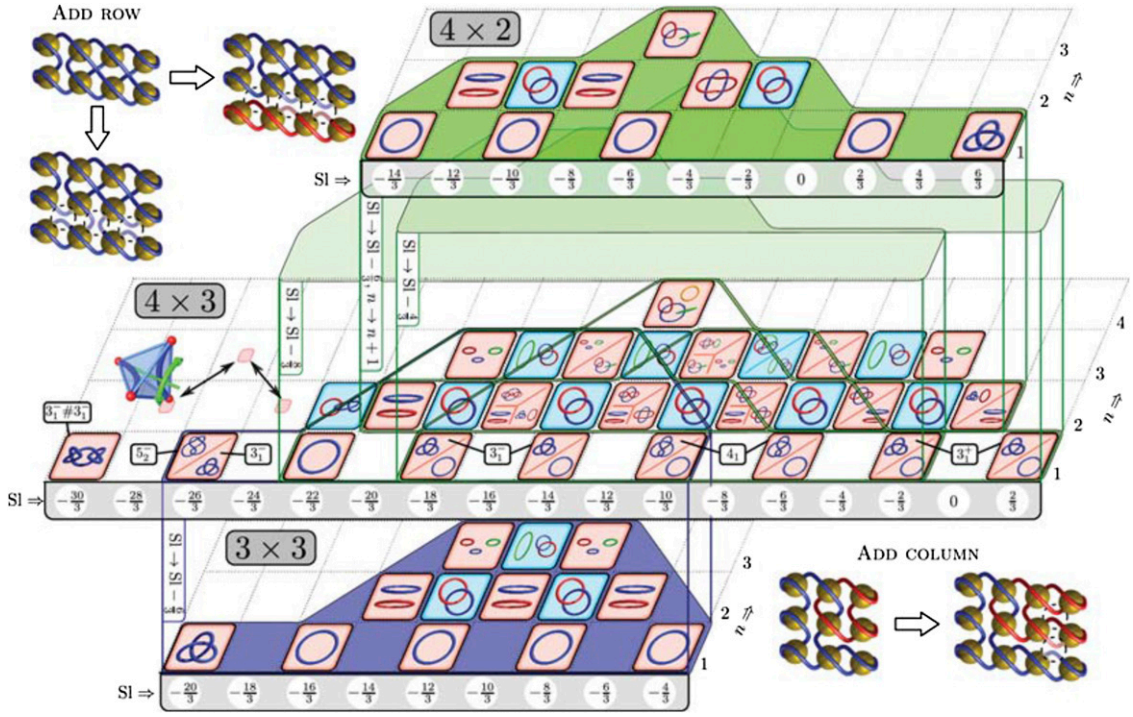

Fig. 5. A diagram classifies all disclination configurations on a 4×3 grid, with marked structures that are just extensions of structures on subgrids of dimensions 3×3 (blue outline) and 4×2 (green outline). Note that the large grid includes structures, not found on smaller grids. The shifts in the Sl from the smaller grids are marked. Linked and unlinked structures are shaded in blue and red, respectively. (*Top Left*) Extending a colloidal grid by one row adds an unlinked loop, which can be attached by changing one tangle to or . Resulting structure has the same knot topology as the original one. (*Bottom Right*) Attached column preserves the knot if all of the added tangles are of type. Linking and orientation preserving rewirings of a single tangle switches between diagonally adjacent structures that form a triangle, as shown on the left side of the main diagram. Chiral single-component knots are marked with a "±" sign according to the sign of the exponent of the highest-order term in the Jones polynomial.

contains multiple copies of even smaller diagrams. Although these subdiagrams represent a significant percentage of all possible structures, they only account for those that can be simplified by removing a column or a row. Unique structures of greater complexity that are absent from the smaller array require all of the tangles to realize the required topology. These are the interesting structures that increase the available complexity and ultimately allow any knot to be created on a sufficiently large array.

Fig. 5 shows a hierarchical decomposition of a 4×3 diagram with outlined subdiagrams. The trapezoidal shape of the diagrams is inherited from the smaller diagrams. As the subdiagrams exist in differently shifted copies, the shape of the trapezoid is a convolution of the shapes of subdiagrams with an elementary "triangle" that describes the diagonal movement in the diagram under application of the tetrahedral rotations (Fig. 5) (40). This, however, excludes the new structures that are not present on the subdiagrams, which can fall outside this estimated outline. In addition, there is weak clustering of knot types on the diagram. Chiral knots prefer the outskirts of the diagram, whereas amphichiral knots reside toward the center. This reflects the coupling between the chirality of the knot and the sign of the linking number, and thus the geometric writhe of the disclination line. Within the imposed geometric constraints, different knots require different amounts of writhing to entangle.

Conclusion

Among physical fields that potentially allow knotting, liquid crystals stand out as the most versatile, allowing the greatest variety and complexity, as well as a fine experimental manipulation. Among many NLC complexes where knots have been observed with POM, we selected the 90° TN cell as an example that reflects many different aspects of knot theory. The colloidal particles create uniformly arranged rewiring sites, with the tangles directly corresponding to the tangles used in knot theory. The tangles, which also reflect the threefold symmetry induced by the underlying topology of the director field, allow a straightforward calculation of the Jones polynomial and associated invariants. Furthermore, with the use of a λ-plate that introduces a color-dependent phase shift, oppositely twisted domains are unveiled as colored areas that correspond to the planar graph associated with the knot projection seen under the microscope, and aid in the construction of the P-T surface. If accompanied by multiphoton fluorescent microscopy experiments, which extract the P-T surface from a real sample, this method allows a direct comparison of the theoretical result with the experiments, either to confirm the prediction or to calibrate the experiment. With the λ-plate POM imaging, the concept of graph coloring is no longer abstract, but manifests experimentally through the optical effects of the TN cell. This system represents the most complex example to date, where the P-T surface can be easily predicted without simulation or director field measurement, and thus offers a platform for testing and developing further theorems about the homotopy of nematic fields (34). As defects regularly delimit domains with a different optical signature, the method can be generalized to other systems with a broken chiral symmetry, as long as the knot crossings or particles do not overlap in the top projection.

Besides the knot-related topological invariants, the disclination loops have their own topological rules to obey. The self-linking number, and essentially the entire matrix of linking numbers for a multicomponent link (27), decorates the plain mathematical knots with an additional internal structure. We demonstrated that the self-linking number and the number of components act as good additional classifiers that allow organized cataloging of the knotted structures. We observe an ordering that weakly couples the self-linking number to the knot type, especially for the chiral knots. Although there is no strict law connecting the knot

topology to the self-linking number, the hierarchy is nevertheless qualitatively observable. Additional statistical analysis could also yield a metric for the average distance between two knots in terms of the number of tetrahedral rewirings. The number of possible structures increases exponentially with the array size, and the (Sl, n) diagram, which can be thought of as the projection of the multidimensional space onto two parameters, becomes less informative. Depending on the hypotheses one wants to test, additional parameters, such as the number of tangles of a particular type, may be used as the axes to test for correlations.

In conclusion, colloidal aggregates in a TN cell reveal how a physical frustration can cause the system to present itself in a form that is especially suited for a selected set of theoretical approaches. The application of topological methods to a physical system requires adaptations on both the theoretical and the experimental sides and provides a rigorous formalism for handling the more complex aspects of the studied material. Unveiling of interesting new features can be expected for many otherwise well-known materials that have yet to be studied with topologically guided algorithms. For abstract branches of knot theory, an experimental realization can be helpful for understanding and finding alternative methods and is not to be disregarded. The ability to observe the theory in action is a nice opportunity both for education purposes as well as clarifying scientific ideas and revealing a different perspective on existing problems.

Materials and Methods

Sample Preparation. We used a dispersion of 5-μm silica microspheres (Bangs Labs) in a NLC pentylcyanobiphenyl (5CB, Nematel). To obtain a homeotropic NLC alignment on the surface of colloidal particles, we have treated the microspheres with 1 wt % aqueous solution of the surfactant *N*-dimethyl-*n*-octadecyl-3-aminopropyl-trimethoxysilyl chloride (DMOAP, ABCR). The colloidal dispersion was confined to wedge-like TN cells, made of 0.7-mm-thick glass plates, coated with transparent indium–tin–oxide and rubbed polyimide alignment layers (PI-2555, Nissan Chemical), spaced by a 6-μm-thick mylar foil. The alignment directions at the top and bottom glass substrates were set perpendicular to ensure a 90° twist of the director. The twist was identified by the colors observed between crossed polarizers with an inserted λ-plate, which shifts the phase of 530-nm light by 2 π.

Experimental Setup. Silica microspheres and defect loops in the NLC were manipulated with laser tweezers setup built around an inverted optical microscope (Nikon, TE-2000) equipped with water immersion objective (Nikor, NIR Apo 60 × /1.0w) and Ar^+ ion laser (Coherent, Innova 90C-4), controlled by a pair of acoustooptic deflectors (Aresis). Laser power was set to 40 mW at the focal point which allowed for effective manipulation. The assembled structures were observed with polarized light microscope (Nikon, E600) and captured with a camera (Nikon, Coolpix E5400).

ACKNOWLEDGMENTS. The authors acknowledge stimulating discussions with B. G. Chen, R. D. Kamien, R. B. Kusner, M. Ravnik, and R. Sazdanović. We thank the Kavli Institute for Theoretical Physics at University of California, Santa Barbara, for their hospitality during the 2012 "Knotted Fields" miniprogram and acknowledge partial support by National Science Foundation (NSF) Grant PHY11-25915. This work was supported by the Slovenian Research Agency under Contracts P1-0099, P1-0055, J1-3612, J1-6723, and Z1-6725, and in part by the Center of Excellence NAMASTE. S.Č. acknowledges support from NSF Materials Research Science and Engineering Centers Grant DMR11-20901.

1. Adams CC (1994) *The Knot Book* (W. H. Freeman and Company, New York).
2. Prasolov VV, Sossinsky AB (1997) *Knots, Links, Braids and 3-Manifolds* (American Mathematical Society, Providence, RI).
3. Cromwell PR (2004) *Knots and Links* (Cambridge Univ Press, Cambridge, UK).
4. Faddeev L, Niemi AJ (1997) Stable knot-like structures in classical field theory. *Nature* 387(6628):58–61.
5. Sutcliffe PM (2007) Knots in the Skyrme-Faddeev model. *Proc R Soc Lond A* 463(2077): 3001–3020.
6. Moffatt HK (1969) The degree of knottedness of tangled vortex lines. *J Fluid Mech* 35: 117–129.
7. Moffatt HK (2014) Helicity and singular structures in fluid dynamics. *Proc Natl Acad Sci USA* 111(10):3663–3670.
8. Scheeler MW, Kleckner D, Proment D, Kindlmann GL, Irvine WT (2014) Helicity conservation by flow across scales in reconnecting vortex links and knots. *Proc Natl Acad Sci USA* 111(43):15350–15355.
9. Kleckner D, Irvine WTM (2013) Creation and dynamics of knotted vortices. *Nat Phys* 9(4):253–258.
10. Herges R (2006) Topology in chemistry: Designing Möbius molecules. *Chem Rev* 106(12):4820–4842.
11. Ayme J-F, Beves JE, Campbell CJ, Leigh DA (2013) Template synthesis of molecular knots. *Chem Soc Rev* 42(4):1700–1712.
12. Han D, Pal S, Liu Y, Yan H (2010) Folding and cutting DNA into reconfigurable topological nanostructures. *Nat Nanotechnol* 5(10):712–717.
13. Micheletti C, Marenduzzo D, Orlandini E (2011) Polymers with spatial or topological constraints: Theoretical and computational results. *Phys Rep* 504(1):1–73.
14. Meluzzi D, Smith DE, Arya G (2010) Biophysics of knotting. *Annu Rev Biophys* 39:349–366.
15. Irvine WTM, Bouwmeester D (2008) Linked and knotted beams of light. *Nat Phys* 4(9):716–720.
16. Kedia H, Bialynicki-Birula I, Peralta-Salas D, Irvine WTM (2013) Tying knots in light fields. *Phys Rev Lett* 111(15):150404.
17. Dennis MR, King RP, Jack B, O'Holleran K, Padgett MJ (2010) Isolated optical vortex knots. *Nat Phys* 6(2):118–121.
18. Hasan MZ, Kane CL (2010) Topological insulators. *Rev Mod Phys* 82(4):3045–3067.
19. Vilenkin A, Shellard EPS (1994) *Cosmic Strings and Other Topological Defects* (Cambridge Univ Press, Cambridge, UK).
20. Mermin ND (1979) The topological theory of defects in ordered media. *Rev Mod Phys* 51(3):591–648.
21. Kurik MV, Lavrentovich OD (1988) Defects in liquid crystals: Homotopy theory and experimental studies. *Sov Phys Usp* 31(3):196–224.
22. Nelson D (2002) *Defects and Geometry in Condensed Matter Physics* (Cambridge Univ Press, Cambridge, UK).
23. Alexander GP, Chen BG, Matsumoto EA, Kamien RD (2012) Colloquium: Disclination loops, point defects, and all that in nematic liquid crystals. *Rev Mod Phys* 84(2):497–514.
24. de Gennes P-G, Prost J (1993) *The Physics of Liquid Crystals* (Oxford Univ Press, Oxford, UK).
25. Poulin P, Stark H, Lubensky TC, Weitz DA (1997) Novel colloidal interactions in anisotropic fluids. *Science* 275(5307):1770–1773.
26. Muševič I, Škarabot M, Tkalec U, Ravnik M, Žumer S (2006) Two-dimensional nematic colloidal crystals self-assembled by topological defects. *Science* 313(5789):954–958.
27. Čopar S (2014) Topology and geometry of nematic braids. *Phys Rep* 538(1):1–37.
28. Smalyukh II, Lansac Y, Clark NA, Trivedi RP (2010) Three-dimensional structure and multistable optical switching of triple-twisted particle-like excitations in anisotropic fluids. *Nat Mater* 9(2):139–145.
29. Chen BG, Ackerman PJ, Alexander GP, Kamien RD, Smalyukh II (2013) Generating the Hopf fibration experimentally in nematic liquid crystals. *Phys Rev Lett* 110(23):237801.
30. Senyuk B, et al. (2013) Topological colloids. *Nature* 493(7431):200–205.
31. Liu Q, Senyuk B, Tasinkevych M, Smalyukh II (2013) Nematic liquid crystal boojums with handles on colloidal handlebodies. *Proc Natl Acad Sci USA* 110(23):9231–9236.
32. Machon T, Alexander GP (2013) Knots and nonorientable surfaces in chiral nematics. *Proc Natl Acad Sci USA* 110(35):14174–14179.
33. Martinez A, et al. (2014) Mutually tangled colloidal knots and induced defect loops in nematic fields. *Nat Mater* 13(3):258–263.
34. Machon T, Alexander GP (2014) Knotted defects in nematic liquid crystals. *Phys Rev Lett* 113(2):027801.
35. Campbell MG, Tasinkevych M, Smalyukh II (2014) Topological polymer dispersed liquid crystals with bulk nematic defect lines pinned to handlebody surfaces. *Phys Rev Lett* 112(19):197801.
36. Araki T, Tanaka H (2006) Colloidal aggregation in a nematic liquid crystal: Topological arrest of particles by a single-stroke disclination line. *Phys Rev Lett* 97(12):127801.
37. Ravnik M, et al. (2007) Entangled nematic colloidal dimers and wires. *Phys Rev Lett* 99(24):247801.
38. Tkalec U, Ravnik M, Čopar S, Žumer S, Muševič I (2011) Reconfigurable knots and links in chiral nematic colloids. *Science* 333(6038):62–65.
39. Jampani VSR, et al. (2011) Colloidal entanglement in highly twisted chiral nematic colloids: Twisted loops, Hopf links, and trefoil knots. *Phys Rev E Stat Nonlin Soft Matter Phys* 84(3 Pt 1):031703.
40. Čopar S, Žumer S (2011) Nematic braids: Topological invariants and rewiring of disclinations. *Phys Rev Lett* 106(17):177801.
41. Čopar S, Clark NA, Ravnik M, Žumer S (2013) Elementary building blocks of nematic disclination networks in densely packed 3D colloidal lattices. *Soft Matter* 9(34): 8203–8209.
42. Seč D, Čopar S, Žumer S (2014) Topological zoo of free-standing knots in confined chiral nematic fluids. *Nat Commun* 5:3057.
43. Tkalec U, Muševič I (2013) Topology of nematic liquid crystal colloids confined to two dimensions. *Soft Matter* 9(34):8140–8150.
44. Scharein RG (1998) Interactive topological drawing. PhD thesis (University of British Columbia, Vancouver).
45. Tkalec U, Škarabot M, Muševič I (2008) Interactions of micro-rods in a thin layer of a nematic liquid crystal. *Soft Matter* 4(12):2402–2409.
46. Brezis H, Coron JM, Lieb EH (1986) Harmonic maps with defects. *Commun Math Phys* 107(4):649–705.
47. Stark H (2001) Physics of colloidal dispersions in nematic liquid crystals. *Phys Rep* 351(6):387–474.
48. Kauffman LH (2001) *Knots and Physics* (World Scientific, Singapore), 3rd Ed.
49. Jablan SV, Radović L, Sazdanović R, Zeković A (2011) Mirror-curves and knot mosaics. arXiv:1106.3784v1.
50. Geiges H (2008) *An Introduction to Contact Topology* (Cambridge Univ Press, Cambridge, UK).